

Magnetic Ordering and Relation to the Metal-Insulator Transition in $\text{Pr}_{1-x}\text{Sr}_x\text{MnO}_3$ and $\text{Nd}_{1-x}\text{Sr}_x\text{MnO}_3$ with $x \sim 1/2$

H. Kawano,¹ R. Kajimoto,² H. Yoshizawa,² Y. Tomioka,³ H. Kuwahara,³ and Y. Tokura^{3,4}

¹The Institute of Physical and Chemical Research (RIKEN), Wako, Saitama 351-01, Japan

²Neutron Scattering Laboratory, I.S.S.P., University of Tokyo, Tokai, Ibaraki 319-11, Japan

³Joint Research Center for Atom Technology (JRCAT), Tsukuba, Ibaraki 305, Japan

⁴Department of Applied Physics, University of Tokyo, Bunkyo-ku, Tokyo 113, Japan

(Received 26 April 1996; revised manuscript received 6 March 1997)

We studied three distorted perovskite manganites, $\text{Pr}_{1/2}\text{Sr}_{1/2}\text{MnO}_3$ and $\text{Nd}_{1-x}\text{Sr}_x\text{MnO}_3$ with $x = 1/2$ and 0.55 by the neutron diffraction technique. Two samples with $x = 1/2$ exhibit a transition from a ferromagnetic (FM) metal to an antiferromagnetic (AFM) nonmetal. We demonstrate that, in the low temperature phase, $\text{Nd}_{1/2}\text{Sr}_{1/2}\text{MnO}_3$ has a CE-type AFM structure with charge ordering, while $\text{Pr}_{1/2}\text{Sr}_{1/2}\text{MnO}_3$ and $\text{Nd}_{0.45}\text{Sr}_{0.55}\text{MnO}_3$ exhibit an A-type layered AFM structure, but show no clear sign of charge ordering. From the present results, we suggest a possible anisotropy of transport as well as magnetic properties in the A-type AFM structure near $x \sim 1/2$. [S0031-9007(97)03224-9]

PACS numbers: 71.27.+a, 71.30.+h, 75.25.+z

Recent discovery of the colossal negative magnetoresistance has attracted a considerable interest on distorted perovskite manganites. As is well known, distorted perovskite manganites such as $\text{La}_{1-x}\text{Sr}_x\text{MnO}_3$ [1] and $\text{La}_{1-x}\text{Ca}_x\text{MnO}_3$ [2-4] undergo a transition from an antiferromagnetic (AFM) insulating state to a ferromagnetic (FM) metallic state by doping carriers. However, the FM metallic state is easily suppressed by the formation of charge ordering. Especially, a commensurate fraction of the carrier concentration such as $1/8$, $1/3$, and $1/2$ is expected to favor a particular type of charge ordering. For example, charge ordering near $x \approx 1/2$ is reported in several systems such as $\text{Pr}_{1-x}\text{Ca}_x\text{MnO}_3$ [5-8], $\text{Pr}_{1/2}\text{Sr}_{1/2}\text{MnO}_3$ [9,10], $\text{Nd}_{1/2}\text{Sr}_{1/2}\text{MnO}_3$ [11], and $\text{La}_{1-x}\text{Ca}_x\text{MnO}_3$ [3,4], and a type of charge ordering in these materials is claimed to be of a CE-type structure as initially named by Wollan and Koehler in Ref. [3].

In Fig. 1, typical behavior of resistivity in a charge ordered system with $x \approx 1/2$ is exemplified by those of $\text{Pr}_{1/2}\text{Sr}_{1/2}\text{MnO}_3$ [10] and $\text{Nd}_{1/2}\text{Sr}_{1/2}\text{MnO}_3$ [11]. Note that both systems exhibit metal-to-nonmetal transitions upon cooling. They become a FM metal below $T_C \sim 250$ K, but transform to an AFM nonmetal at $T_N \sim 150$ K. A salient feature of their resistivity is a drastic difference of the behavior below T_N , despite their having very similar T_C 's and T_N 's. The resistivity of $\text{Nd}_{1/2}\text{Sr}_{1/2}\text{MnO}_3$ shows a dramatic increase at T_N , and continues to increase upon cooling ($R \sim 1.6 \times 10^2 \Omega \text{ cm}$ at 5 K). By contrast, the resistivity of $\text{Pr}_{1/2}\text{Sr}_{1/2}\text{MnO}_3$ shows an increase at T_N , but remains a relatively low value down to 5 K ($R \sim 1.8 \times 10^{-2} \Omega \text{ cm}$ at 5 K, being 4 orders of magnitude smaller than the resistivity of the Nd compound). To elucidate such a distinct difference in the resistivity, it seems to be important to gain profound understanding of the nature of the charge ordering state in these manganites. These considerations motivated us to investigate their magnetic and structural behavior utilizing the neu-

tron diffraction technique. For this purpose, we chose three samples, $\text{Pr}_{1/2}\text{Sr}_{1/2}\text{MnO}_3$ and $\text{Nd}_{1-x}\text{Sr}_x\text{MnO}_3$ with $x = 1/2, 0.55$. We note that $\text{Nd}_{0.45}\text{Sr}_{0.55}\text{MnO}_3$ orders antiferromagnetically at $T_N = T_S = 225$ K with a first order structural transition. Its resistivity shows a sharp increase at T_N . But, interestingly, it remains a very low value of $4.0 \sim 5.0 \times 10^{-3} \Omega \text{ cm}$ before it shows an upturn below 80 K (not shown), similar to $\text{Pr}_{1/2}\text{Sr}_{1/2}\text{MnO}_3$.

For CE-type charge ordered manganites with $x \approx 1/2$, the CE-type AFM spin structure due to a specific arrangement of e_g orbitals is also presumed. In the present study, however, we found that $\text{Pr}_{1/2}\text{Sr}_{1/2}\text{MnO}_3$ and $\text{Nd}_{0.45}\text{Sr}_{0.55}\text{MnO}_3$ samples exhibit a layered A-type AFM ordering. We suggest that a wider one-electron band width may

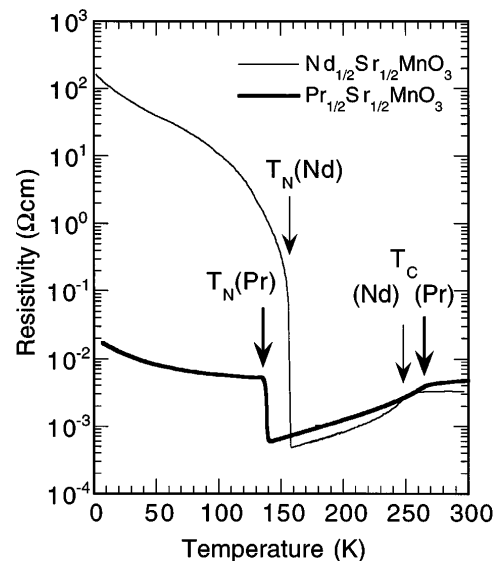


FIG. 1. Temperature dependence of the resistivity of $\text{Pr}_{1/2}\text{Sr}_{1/2}\text{MnO}_3$ and $\text{Nd}_{1/2}\text{Sr}_{1/2}\text{MnO}_3$. Thick and thin arrows denote transition temperatures for Pr and Nd manganites, respectively.

suppress the CE-type charge ordering in the samples with $x \approx 1/2$, and then it favors the A-type AFM ordering.

Single crystal samples were melt grown by the floating-zone method. The details of a sample preparation method were reported in the previous papers [10,11]. We checked the stoichiometry of the samples by electron-probe microanalysis, ICP-MS, and iodometric titration, and the results show that our samples agree with a nominal concentration within a 1% accuracy.

Neutron diffraction measurements were performed with triple axis spectrometers GPTAS, HQR, and HER installed at the JRR-3M research reactor in JAERI, Tokai, Japan. Neutrons with incident momentum of $k_i = 2.57 \text{ \AA}^{-1}$ were obtained by the (002) reflection of the pyrolytic graphite monochromator, and a combination of $40'-20'-20'$ collimators was utilized for profile measurements on GPTAS, while collimation was relaxed to $40'-40'-40'$ for measurements of the temperature dependence of the integrated intensities.

We briefly summarize the temperature dependence of magnetic behavior of three samples by showing that of magnetic Bragg reflections in Fig. 2. Two samples with $x = 1/2$, $\text{Pr}_{1/2}\text{Sr}_{1/2}\text{MnO}_3$ and $\text{Nd}_{1/2}\text{Sr}_{1/2}\text{MnO}_3$, show FM ordering in the intermediate phase for $T_C > T > T_N$,

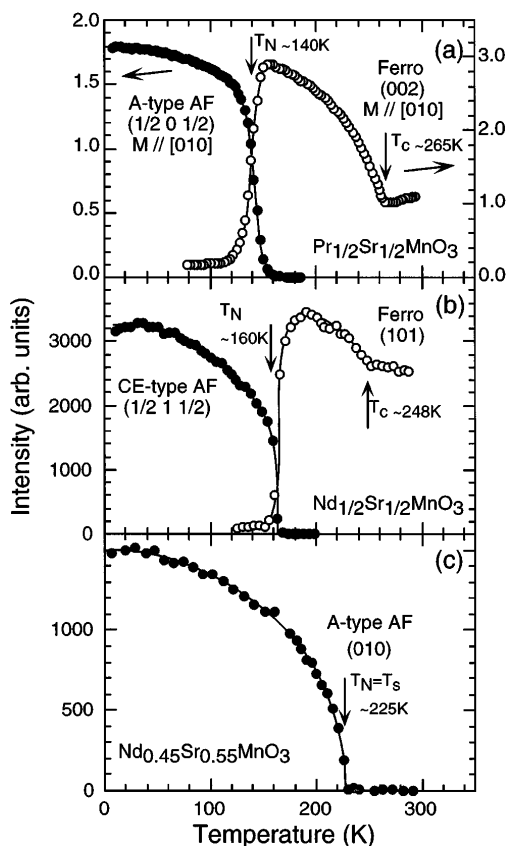


FIG. 2. Temperature dependence of magnetic Bragg reflections in three samples. Integrated intensities were measured through a $\theta - 2\theta$ scan.

and they enter an AFM state below T_N as shown in Figs. 2(a) and 2(b), respectively. The third sample $\text{Nd}_{0.45}\text{Sr}_{0.55}\text{MnO}_3$ exhibits AFM ordering below $T_N = T_S = 225 \text{ K}$ as shown in Fig. 2(c). In the low temperature phase, all three samples have the AFM ordering.

In contrast to our expectation of the CE-type AFM spin structure accompanied with the well-established charge ordering for the samples with $x \approx 1/2$, we have discovered that $\text{Pr}_{1/2}\text{Sr}_{1/2}\text{MnO}_3$ and $\text{Nd}_{0.45}\text{Sr}_{0.55}\text{MnO}_3$ samples exhibit a different magnetic structure in their AFM phases. The difference of magnetic structures in three samples is best contrasted by their neutron powder diffraction patterns shown in Fig. 3. Shaded peaks in Fig. 3 indicate AFM superlattice peaks. By comparing three panels, one can easily see that magnetic structures of $\text{Pr}_{1/2}\text{Sr}_{1/2}\text{MnO}_3$ and $\text{Nd}_{0.45}\text{Sr}_{0.55}\text{MnO}_3$ are qualitatively identical, but are different from that of $\text{Nd}_{1/2}\text{Sr}_{1/2}\text{MnO}_3$. Indeed, the powder pattern of $\text{Nd}_{1/2}\text{Sr}_{1/2}\text{MnO}_3$ can be indexed by the CE-type AFM structure as is proposed by previous studies [11]. We found, however, that the patterns of $\text{Pr}_{1/2}\text{Sr}_{1/2}\text{MnO}_3$ and $\text{Nd}_{0.45}\text{Sr}_{0.55}\text{MnO}_3$ should be indexed with an A-type AFM structure similar to those in LaMnO_3 [3] and lightly doped $\text{La}_{1-x}\text{Sr}_x\text{MnO}_3$ [12].

We should note that a previous neutron scattering study by Knizek *et al.* [9] showed that their $\text{Pr}_{1/2}\text{Sr}_{1/2}\text{MnO}_3$ sample had the CE-type AFM structure in its low temperature phase. We have studied several samples of the $\text{Pr}_{1-x}\text{Sr}_x\text{MnO}_3$ system with $0.45 < x < 0.55$, but found that none of them exhibits a CE-type AFM phase. We note that our powder sample was prepared by grinding melt

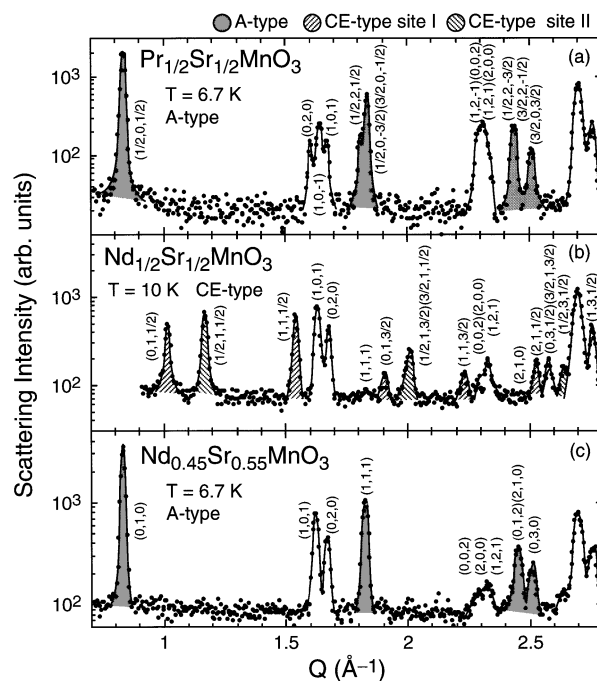


FIG. 3. Portion of powder profiles in the low temperature phase of three samples. Shaded area indicates magnetic contributions.

grown single crystals, while their sample was prepared by the solid state reaction method. In order to elucidate the discrepancy of the magnetic structure for $\text{Pr}_{1/2}\text{Sr}_{1/2}\text{MnO}_3$ between two groups, we have prepared a calcined polycrystalline sample by the solid state reaction method and examined its magnetic structure. Being consistent with our melt-grown samples, our calcined polycrystalline sample also showed the *A*-type AFM structure, although the AFM transition was drastically broadened. Therefore, we conclude that $\text{Pr}_{1/2}\text{Sr}_{1/2}\text{MnO}_3$ has the *A*-type AFM structure, and the different magnetic structure in the preceding study should be attributed to a slight off-stoichiometry (different *x* and/or oxygen content).

For the CE-type magnetic structure, Mn^{3+} and Mn^{4+} ions are believed to form the $(\pi, 0, \pi)$ -type charge ordering [13]. As evidence for the CE-type charge ordering in $\text{Nd}_{1/2}\text{Sr}_{1/2}\text{MnO}_3$, we observed superlattice reflections which correspond to a doubling of the unit cell along the *c* direction due to a specific arrangement of e_g orbitals in the CE-type charge ordering. On the other hand, in the *A*-type AFM case of $\text{Pr}_{1/2}\text{Sr}_{1/2}\text{MnO}_3$ and $\text{Nd}_{0.45}\text{Sr}_{0.55}\text{MnO}_3$, we have made a systematic search of charge ordering peaks in single crystal samples, but found no evident indication of charge ordering. We emphasize here, however, that the two magnetic structures at $x \sim 1/2$ observed in the present study are beautifully correlated with distinctly different behavior of the resistivity in the AFM phase shown in Fig. 1.

In the present two samples, $\text{Nd}_{1/2}\text{Sr}_{1/2}\text{MnO}_3$ and $\text{Pr}_{1/2}\text{Sr}_{1/2}\text{MnO}_3$, the hole concentration n_h is held fixed at $n_h = 1/2$. Therefore, the replacement of Nd ions with

larger Pr ions causes an increase of the tolerance factor. In other words, the substitution widens the one-electron bandwidth (*W*), leading to a strong enhancement of the itinerant character of e_g electrons in the $\text{Pr}_{1/2}\text{Sr}_{1/2}\text{MnO}_3$ system. With the increase of *W*, the double exchange (DE) mechanism may allow metallic conductivity within FM layers in the *A*-type AFM structure through gain of kinetic energy for e_g electrons. We consider that such a change of *W* can be an origin of the *A*-type AFM structure. It is relevant to mention the recent study on the $(\text{Nd}_{1-z}\text{La}_z)_{1/2}\text{Sr}_{1/2}\text{MnO}_3$ system [14]. In this study, influence of *W* on the transport properties was studied for a fixed hole concentration $n_h = 1/2$. Interestingly, another AFM phase was suggested in between the CE-type AFM phase and the FM metallic phase. These results can be understood as a consequence of the reduction of *W*. For the $n_h = 1/2$ system, the CE-type charge ordering is realized when the system has a small *W*, while with the increase of *W*, the CE-type charge ordering is progressively suppressed, and surprisingly, the layered *A*-type AFM phase can be favored before the FM metallic state is established.

Finally, we point out that the *A*-type magnetic structure also affects the crystal structure. We have performed a standard Rietveld refinement analysis of our powder pattern data [15], and part of the results on the magnetic and lattice structures are summarized in Table I. Interesting quantities in these crystal structures are Mn-O-Mn bond angles along the *b* direction and within the *ac* plane, and they are listed in the columns Θ_b and Θ_{ac} . There is a clear correlation between the Mn-O-Mn bond angles and the *A*-type AFM structure. In the case of the

TABLE I. Magnetic structure (MS), moments, the direction of magnetic moment, lattice constants, and Mn-O-Mn bond angles determined from Rietveld analysis of powder profile data. In the column of MS, symbols F, A, and CE denote the ferromagnetic, *A*-type AFM, and CE-type AFM structures, respectively. Θ_b and Θ_{ac} denote the Mn-O-Mn bond angles along the *b* axis and within the *a-c* plane.

	<i>T</i> (K)	MS	Moment		(μ_B)	<i>a</i> (Å)	<i>b</i> /√2 (Å)	<i>c</i> (Å)	Mn-O-Mn (deg.)		
									Θ_b	Θ_{ac}	Θ_{ac}
$\text{Pr}_{1/2}\text{Sr}_{1/2}\text{MnO}_3$	6.7	A	3.1		[010]	5.362(4)	5.531(2)	5.371(3)	171.6(2.5)	163.1(3.0) ^a	161.4(3.0) ^a
	110	A	3.0		[010]	5.360(3)	5.525(2)	5.377(3)	175.9(2.5)	165.4(3.0) ^a	162.2(3.0) ^a
	170	F	2.8		[010]	5.380(1)	5.505(1)	5.408(1)	158.2(3.0)	171.4(3.0)	
	276	P				5.382(1)	5.509(1)	5.420(1)	157.9(2.5)	170.6(2.5)	
$\text{Nd}_{1/2}\text{Sr}_{1/2}\text{MnO}_3$	10	CE	3.0 ^b	2.8 ^b	[001] ^c	5.445(1)	5.326(1)	5.515(1)	161.8(2.0)	161.9(2.0)	
	155	CE	1.9 ^b	1.8 ^b	[001] ^c	5.442(1)	5.331(2)	5.504(1)	162.1(2.8)	161.9(2.5)	
	174	F	2.6		[001]	5.423(1)	5.397(1)	5.469(1)	162.7(1.7)	167.2(2.5)	
	296	P				5.434(1)	5.398(1)	5.477(1)	159.6(2.5)	168.2(2.5)	
$\text{Nd}_{0.45}\text{Sr}_{0.55}\text{MnO}_3$	6.7	A	3.0		[001]	5.440(1)	5.312(1)	5.494(1)	161.8(4.0)	168.3(2.0)	
	180	A	2.5		[001]	5.437(1)	5.324(1)	5.491(1)	161.8(3.5)	168.1(2.0)	
	250	P				5.360(2)	5.498(2)	5.413(2)	156.7(2.5)	170.6(3.0)	

^aThe lattice structure of $\text{Pr}_{1/2}\text{Sr}_{1/2}\text{MnO}_3$ in the *A*-type AFM phase is $P21/n$. The bond angles in the *a-c* plane in the monoclinic $P21/n$ phase are not identical. The values in the first and second columns give the angles along the [101] and $[10\bar{1}]$ directions, respectively.

^bFor the CE-type AFM structure, the first and second columns give the magnetic moments for the Mn^{3+} and Mn^{4+} sites (site I and II), respectively.

^cThis direction is for Mn^{3+} (site I) and the direction of magnetic moment for Mn^{4+} (site II) is not determined.

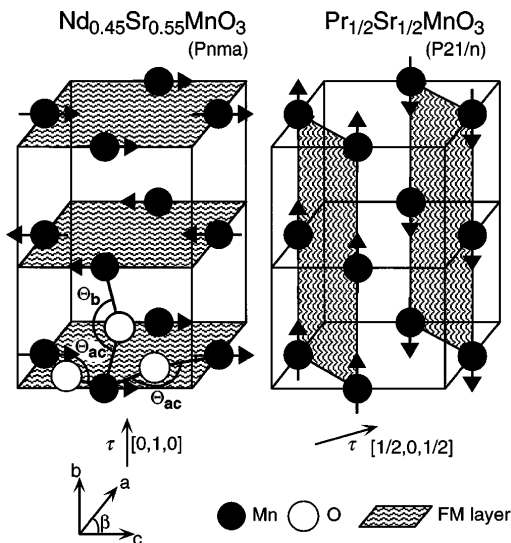


FIG. 4. A-type layered AFM structure and its propagation vector τ for the orthorhombic $\text{Nd}_{0.45}\text{Sr}_{0.55}\text{MnO}_3$ and the monoclinic $\text{Pr}_{1/2}\text{Sr}_{1/2}\text{MnO}_3$.

CE-type AFM phase of $\text{Nd}_{1/2}\text{Sr}_{1/2}\text{MnO}_3$, the Mn-O-Mn bond angles along the three directions are almost identical, being $\sim 162^\circ$. On the other hand, in the case of the A-type AFM phase of $\text{Nd}_{0.45}\text{Sr}_{0.55}\text{MnO}_3$, the bond angles within the FM layers $\Theta_{ac} \sim 168^\circ$ are substantially larger than those between the FM layers $\Theta_b \sim 162^\circ$. A similar trend is also found in $\text{Pr}_{1/2}\text{Sr}_{1/2}\text{MnO}_3$. This sample has a monoclinic $P21/n$ structure in the AFM phase [16]. The monoclinic distortion causes the change of the propagation vector, τ , of the A-type AFM structure from the $[0, 1, 0]$ direction in the case of $Pnma$ structure to the $[1/2, 0, 1/2]$ direction as depicted in Fig. 4. Nevertheless, the largest Mn-O-Mn bond angle still lies in the FM layers. This systematic difference of the Mn-O-Mn bond angles in the A-type AFM structure might cause an anisotropy of transport and magnetic properties within and perpendicular to the FM layers. We also comment that the DE mechanism further favors an anisotropy of resistivity within and perpendicular to the FM layers in the A-type spin structure.

In conclusion, we studied three distorted perovskite manganites, $\text{Pr}_{1/2}\text{Sr}_{1/2}\text{MnO}_3$ and $\text{Nd}_{1-x}\text{Sr}_x\text{MnO}_3$ with

$x = 1/2$ and 0.55, and demonstrated that there exists a close correlation among the magnetic, crystal structures and the transport properties. We suggest that the A-type AFM ordering which appears in a limited region with $x \sim 1/2$ certainly deserves further studies, including their possible anisotropies on magnetic and transport properties. It is also interesting to investigate theoretically in what case the A-type ordering is stabilized against the FM ordering.

This work was supported by a Grant-In-Aid for Scientific Research from the Ministry of Education, Science and Culture, Japan, by Special Researcher's Basic Science Program (RIKEN), and by the New Energy and Industrial Technology Development Organization (NEDO) of Japan.

- [1] Y. Tokura *et al.*, J. Phys. Soc. Jpn. **63**, 3931 (1994); A. Urushibara *et al.*, Phys. Rev. B **51**, 14 103 (1995), and references cited therein.
- [2] G.H. Jonker and J.H. van Santen, Physica (Utrecht) **16**, 337 (1950).
- [3] E.O. Wollan and W.C. Koehler, Phys. Rev. **100**, 545 (1955).
- [4] P. Schiffer *et al.*, Phys. Rev. Lett. **75**, 3336 (1995); P.G. Radaelli *et al.*, *ibid.* **75**, 4488 (1995), and references cited therein.
- [5] Z. Jirak *et al.*, J. Magn. Magn. Mater. **15-18**, 519 (1980); **53**, 153 (1985).
- [6] E. Pollert *et al.*, J. Phys. Chem. Solids **43**, 1137 (1982).
- [7] Y. Tomioka *et al.*, J. Phys. Soc. Jpn. **64**, 3626 (1995); Phys. Rev. B **53**, R1689 (1996).
- [8] H. Yoshizawa *et al.*, Phys. Rev. B **52**, R13 141 (1995); J. Phys. Soc. Jpn. **65**, 1043 (1996).
- [9] K. Knizek *et al.*, J. Solid State Chem. **100**, 292 (1992).
- [10] Y. Tomioka *et al.*, Phys. Rev. Lett. **74**, 5108 (1995).
- [11] H. Kuwahara *et al.*, Science **270**, 961 (1995).
- [12] H. Kawano *et al.*, Phys. Rev. B **53**, 2202 (1996); **53**, R14 709 (1996).
- [13] J.B. Goodenough *et al.*, Phys. Rev. **124**, 373 (1961).
- [14] Y. Moritomo *et al.*, Phys. Rev. B **55**, 7549 (1997).
- [15] Y.-I. Kim and F. Izumi, J. Ceram. Soc. Jpn. **102**, 401 (1994).
- [16] Note that the nuclear Bragg peaks (101) and (020) are split into three peaks in the monoclinic phase of $\text{Pr}_{1/2}\text{Sr}_{1/2}\text{MnO}_3$ as seen in Fig. 3(a).